Grain-boundary atomic structure in nanocrystalline palladium from x-ray atomic distribution functions

Jörg Löffler* and Jörg Weissmüller†
Fachbereich 15 and Institut für Neue Materialien, Universität des Saarlandes, 66041 Saarbrücken, Germany
(Received 28 December 1994)

We discuss the scattering theory of nanocrystalline solids, based on an evaluation of the intragrain and intergrain parts of the atomic distribution function. The results are applied to experimental x-ray scattering data obtained on a set of nanocrystalline Pd samples, prepared by inert-gas condensation, with different consolidation, aging, and annealing parameters. The experimental results show that the number of atomic neighbors in the crystal lattice coordination shells of nanocrystalline Pd is substantially lower than the one in the coarse-grained polycrystal lattice. The findings suggest that as a function of their age and thermal treatment, the samples have two different atomic structures. In samples aged for several months at room temperature, and in annealed samples, practically all atoms are located on crystal lattice sites, and the reduction in nearest-neighbor coordination number is an effect of the finite size of the crystallites. In fine-grained samples examined within 10 days of preparation, about 10% of the atoms are located on nonlattice sites with little or no atomic short-range order. This corresponds to about two atomic monolayers of atoms on nonlattice sites at the grain boundaries in as-prepared samples, as compared to about one-quarter of a monolayer in aged or annealed samples. The distribution of nearest-neighbor interatomic spacings for atoms on crystal lattice sites in nanocrystalline Pd is not measurably widened compared to the one of coarse-grained reference samples, indicating that disorder in the crystal lattice, as probed by the x-ray Debye-Waller parameter, involves displacements correlated over several lattice parameters, rather than short-range, uncorrelated atomic displacements.

I. INTRODUCTION

Since the earliest studies of nanocrystalline pure metals,[1,2] the motivation for the work has been twofold. First, one is interested in the novel overall properties of these materials, which are determined by their high density of topological defects, specifically grain boundaries. Second, because of this same important contribution of the grain boundaries to the overall properties, nanocrystalline metals provide an opportunity to investigate the grain boundaries themselves by volume-sensitive methods. In contrast to the case of nanocrystals, the low interface-to-bulk signal ratio prevents the application of most volume-sensitive methods to coarse-grained metals. Consequently, there is a considerable interest in the additional data on grain-boundary properties in metals that may be obtained from investigations of nanocrystals.

On the other hand, the first x-ray-diffraction study of nanocrystalline pure Fe (Ref. 3) indicates that the grain boundaries in this material exhibit a strongly reduced local atomic short-range order, suggesting that grain boundaries in nanocrystals may be of a different character from those in conventional coarse-grained polycrystals. A numer of experiments by diffraction,[4,5] spectroscopic,[6–8] and imaging techniques[9,10] provide contradicting evidence on this issue. This has given rise to a controversy in the literature,[4,11] which in a simplistic way may be brought down to the question: Are pure nanocrystalline metals just very fine-grained polycrystals, or is there a qualitative change in the atomic configurations and in the properties of the grain boundaries when the grain size is reduced to the nanometer region?

In the original study of inert-gas condensed nanocrystalline Fe by x-ray diffraction, Zhu and others[3] find an increased diffuse background in the scattering intensity between the Bragg reflections. In a numerical simulation matched to the experimental scattering data, the three outer atomic layers of each crystallite are disordered, with random atomic displacements of 50% of the nearest-neighbor distance in the outermost layer. This result does not seem very realistic in view of the immense energies involved by the resulting overlap of atoms in that layer, and may invite speculation as to the extent of disordered oxide formation at the surfaces and grain boundaries of the 70% (relative to bulk) dense samples produced by early inert-gas methods. In fact, a current high vacuum *in situ* x-ray study for nanocrystalline Fe (Ref. 12) indicates much smaller diffuse intensity. In addition, an x-ray investigation of nanocrystalline Pd, which is less prone to oxidation than Fe, does not reveal an increase in diffuse background,[4] a finding which has been interpreted in terms of an ordered grain-boundary structure[4] in that material. On the other hand, the interpretation of the scattering data has been disputed,[11] and the contrasting results have also been speculated to be due to the different lattice symmetries, in analogy to the different dislocation core structures in bcc and fcc metals.[11] The interpretation of the Pd x-ray data in terms of ordered grain boundaries is apparently supported by high-resolution transmission electron microscopy (HRTEM) data,[9] displaying narrow and facetted grain boundaries in *n*-Pd and *n*-Cu. However, such studies have remained inconclusive because of the difficulties in

estimating the influences of sample preparation on the grain-boundary structure. Rigid body displacements of the crystallites in and perpendicular to the grain-boundary plane are essential for minimizing the grain-boundary energy.[13] In nanocrystalline solids, these displacements are subject to constraints imposed by the surrounding crystals. For observation by HRTEM, the sample is thinned to a thickness of the order of one grain diameter. This process eliminates the constraints, and may thereby induce a relaxation towards a more ordered grain-boundary structure with lower energy. The proposed ordered state of grain boundaries in *n*-Pd contrasts with extended x-ray absorption fine-structure (EXAFS) data which evidence a strong reduction in atomic nearest-neighbor coordination number in that material[6] as well as in other fcc (Ref. 6) and bcc (Ref. 7) nanocrystalline metals.

The assessment of the results is complicated by two factors: First, the characteristics of specimens prepared under supposedly identical conditions vary markedly, partly due to variations in the crystallite size distribution achieved by the inert-gas condensation procedure, and partly due to the recently found dependence of sample properties, including the specific grain-boundary energy, on consolidation parameters,[14] room-temperature aging,[15] and annealing.[16] Recently, it was pointed out that the single sample characteristic reported in many studies, an average grain size value obtained from Bragg reflection full width at half maximum (FWHM) based criteria, does not adequately account for the distribution of grain sizes and for the change of the distribution upon aging or annealing.[17,18] In addition, this sample characteristic cannot account for changes of the energetics (and therefore the atomic structure) of the grain boundaries during annealing. Second, while some of the strongest arguments rest on x-ray data or on EXAFS atomic distribution functions, little effort has been made at quantifying the contribution of grain boundaries in polycrystals on the x-ray interference function or on the atomic distribution function from a theoretical point of view. These factors may account for the controversy over the questions: in how far is the grain-boundary structure of nanocrystalline solids different from the one in conventional polycrystals, to what extent can scattering experiments characterize qualitative details of the grain-boundary structure in nanocrystals, and what quantitative information can be obtained?

In this paper, we address these open questions by discussing the relevant scattering theory, and by comparing the results to experimental atomic distribution functions obtained from a set of *n*-Pd samples with different grain size, preparation, age, and annealing states. Increased interest in this type of analysis arises from the fact that atomic distribution functions are readily computed from atomistic models of nanocrystalline solids generated by molecular-dynamics simulations. Such calculations are presently being carried out by several groups of scientists.[19–21] Comparisons of the experimental data to those obtained from computer-generated models may improve the understanding of the atomic structure and physical properties of nanocrystalline materials.

II. SCATTERING BY SMALL PARTICLES AND NANOCRYSTALS

A. General formalism

For spherically symmetric arrangements of identical atoms, the atomic distribution function[22] $\rho_{(r)}$ contains all the information comprised in the scattering pattern. By definition, $\rho_{(r)}$ is the spherical average of the denisty of atoms surrounding an average central atom at a distance r.[23] For a single-component system, the kinematical scattering theory relates the interference function $P_{(k)}$ (Ref. 24) to $\rho_{(r)}$ by

$$P_{(k)}=\frac{1}{k}\int_{r=0}^{\infty} G_{(r)} f^{\infty} G_{(r)} \sin(kr)dr \tag{1}$$

and its back transform

$$G_{(r)}=\frac{2}{\pi}\int_{k=0}^{\infty} kP_{(k)} \sin(kr)dk \ . \tag{2}$$

Here k is the scattering vector, which is related to the scattering angle, 2θ, and to the wavelength λ, by $k=4\pi \sin(\theta)/\lambda$, and $G_{(r)}$ is the reduced atomic distribution function:

$$G_{(r)}=4\pi r(\rho_{(r)}-\langle\rho\rangle) \tag{3}$$

with $\langle\rho\rangle$ the macroscopic atomic density of the sample. The coherently scattered x-ray intensity is

$$I_{(k)}=V\langle\rho\rangle ff^{*}(P_{(k)}+1) \ . \tag{4}$$

V is the sample volume; f and f^{*} denote the atomic form factor and its complex conjugate. Except for the thermal diffuse background (which is small at low k), $P_{(k)}=-1$ and $I_{(k)}=0$ in coarse-grained polycrystalline, defect-free matter in the k region between the Bragg reflections.

B. Atomic distribution and interference functions of arrays of *nm* particles

In an array of isolated particles, or of crystal grains in a polycrystal, the atomic distribution function can be expressed as the sum of an "intragrain" part, consisting of contributions from pairs of atoms located in the same particle, and of an "intergrain" part, accounting for the remaining interatomic spacings.[18] These two parts can be discussed in a relatively concise form, if the array of particles meets two conditions: first, there must be a spatial arrangement of atoms, with a volume much larger than the particle size, which is homogeneous and, except for simple rigid-body translation and rotation, on a scale of the particle size identical to the arrangement of atoms in the particles. This implies that the intragrain part of the atomic distribution function in the particulate system contains only those interatomic spacings which occur also in the extended structure; it is only the number of the spacings which is reduced due to the finite size of the particles (see Fig. 1). Second, the distribution of the orientations of the crystal lattices (or of any distinguished direction in a noncrystalline system) in different particles must be random. In other words, it is required that all

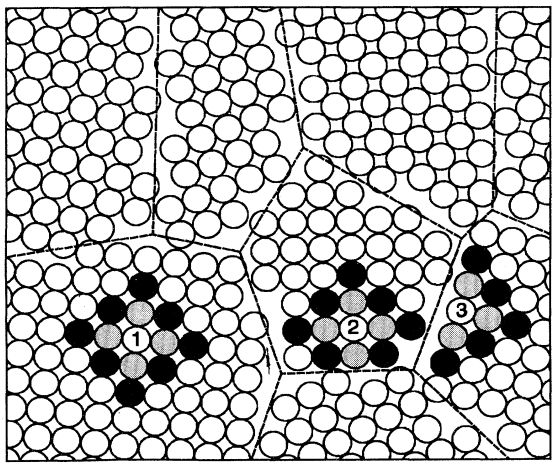

FIG. 1. Schematic illustration of the loss in lattice site atomic neighbor coordination number due to size effect in small particles and nanocrystals. Atom 1, located far from a grain boundary, retains full first- (light shaded circle), second- (dark shaded), and third- (black) nearest-neighbor coordination. Atoms closer to grain boundaries lose part of their third- (atom 2) or first-, second-, and third- (atom 3) nearest neighbors.

orientations occur with the same frequency, and that neighboring particles have no systematic correlation with respect to the relative orientation of their crystal lattices. This condition will be seen to imply the absence of interference related to atomic-scale structure in the intergrain part of the atomic distribution function.

A system which meets the above conditions can be constructed in the following way: in a first step, define geometrical objects, the location in space and the external shape of which delimits the particles. In a second step, inscribe a crystal lattice into each particle. To do so, superimpose the extended lattice, rotated and displaced at random, to the particle, and define the atomic positions in the particle as those atomic positions of the extended lattice which are located inside the particle. Because all atoms, including those in the outer atomic layer of each crystallite, occupy lattice positions, in other words the surface or grain-boundary regions are not reconstructed, the model will be referred to as the "nonreconstructed nanocrystal" model.

Due to the randomness of the construction of the model, the probability of finding a neighboring atom at a distance r from a central atom *in the same particle* is the product of the probability of finding a neighbor at r in the extended lattice, $4\pi r^2\rho^V_{(r)}dr$, and the probability that the respective atom is located inside the particle. The latter quantity is given by the intragrain correlation function of the system. For each point $\mathbf{R}$ in a particle, there is a quantity $H_{(\mathbf{R},r)}$, which specifies the fraction contained within the particle of a spherical shell of radius r centered on a scatterer at $\mathbf{R}$. The intragrain correlation function $H_{(r)}$ is the average of $H_{(\mathbf{R},r)}$ over all $\mathbf{R}$ in all particles. Hence, the intragrain part of the atomic distribution function is $\rho^V_{(r)}H_{(r)}$ (Ref. 25) [see Figs. 1 and 2(a)–2(c)]. The intragrain correlation function is discussed in Refs. 23 and 26. A description of its application for sets of particles with a distribution of sizes is given in Ref. 18. The formalism derived in Ref. 18 is generalized below to include the relation between the atomic short-range order in the grain boundaries and the atomic distribution function.

With respect to the intergrain part of the atomic distribution function, the following is noted: For any given central atom, the *a priori* probability of finding an atom in a small volume dV at a distance $\mathbf{r}$ in a neighboring particle has the same value, $\langle\rho\rangle^V dV$, everywhere in that particle. This results from the fact that the lattices of the neighboring particles are rotated and displaced at random, so that the positions of atoms in neighboring particles cannot be predicted. Consequently, the intergrain part of the atomic distribution function exhibits no atomic-scale structure, and can be expressed as the product of the average density inside the particles, $\langle\rho\rangle^V$, and a function $H'_{(r)}$. $H'_{(r)}$ gives the probability that a volume element located at a distance r from a randomly chosen central atom inside a particle will be located inside a particle different from the one containing the central atom. $H'_{(r)}$ is obtained in a way analogous to $H_{(r)}$: for each point $\mathbf{R}$ in a particle, the quantity $H'_{(\mathbf{R},r)}$ specifies the fraction contained within different particles of a spherical shell of

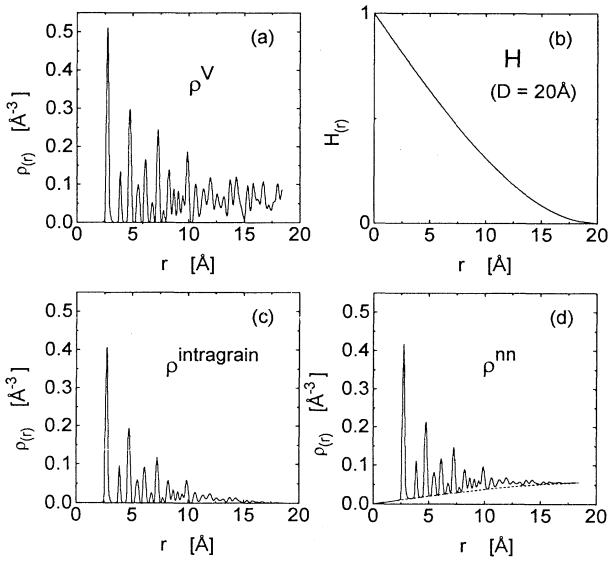

FIG. 2. Schematic illustration of the atomic distribution function in a system of particles: (a) The atomic distribution function of the extended crystal lattice, ρ^V. (b) The intragrain correlation function H for a spherical particle with diameter 20 Å (Ref. 18). (c) The atomic distribution function of the isolated particle is the intragrain part of the total atomic distribution function: $\rho^{\text{intragrain}}_{(r)}=\rho^V_{(r)}H_{(r)}$. (d) The atomic distribution of the nonreconstructed, dense polycrystal model, ρ^{nn} (solid line; compare Sec. II B) is the sum of $\rho^{\text{intragrain}}_{(r)}$ and of the intergrain part, $\langle\rho\rangle^V(1-H_{(r)})$ (dashed line) of the atomic distribution function.

radius r centered on a scatterer at $\mathbf{R}$, and $H'_{(r)}$ is the average of $H'_{(\mathbf{R},r)}$ over all $\mathbf{R}$ in all particles. Intergrain correlation functions for a number of model microstructures are given in Ref. 26.

The total atomic distribution function of the nonreconstructed nanocrystal model, ρ^{nn}, is the sum of intragrain and intergrain parts [see the schematic illustration in Fig. 2(d)]:

$$\rho^{nn}_{(r)}=\rho^{V}_{(r)}H_{(r)}+\langle\rho\rangle^{V}H'_{(r)} \ . \tag{5}$$

An important property of the intragrain correlation function is the following (see the Appendix): independent of the shape of the particles, H decreases linearly from the value unity at $r=0$, with an initial slope which is proportional to the specific free surface area of the particle, $\alpha_S=A/V_P$, with V_P the total volume occupied by all particles, and A the total free surface area of a set of isolated particles with the same size and shape as the particles in the actual system:[27]

$$H_{(r)}=1-\frac{\alpha_S}{4}r \quad (r\ll D) \ . \tag{6}$$

If the particles in the set are geometrically similar, then α_S is proportional to the inverse of the area-weighted average grain size, $\langle D\rangle_{\text{area}}$. For spherical particles, $\alpha_S=6\langle D\rangle^{-1}_{\text{area}}$. The topic of weighted averages of the size distribution is discussed in more detail in Refs. 17 and 18. In polycrystals, as two particle surfaces combine to form a single grain boundary, the specific grain-boundary area is half the specific surface area: $\alpha_{GB}=3\langle D\rangle^{-1}_{\text{area}}$.

With Eq. (3), the reduced atomic distribution function of the array of particles or grains is

$$\begin{aligned}G^{nn}_{(r)}&=4\pi r(\rho^{V}_{(r)}H_{(r)}+\langle\rho\rangle^{V}H'_{(r)}-\langle\rho\rangle)\\&=G^{V}_{(r)}H_{(r)}+4\pi r\langle\rho\rangle^{V}\left[H_{(r)}+H'_{(r)}-\frac{\langle\rho\rangle}{\langle\rho\rangle^{V}}\right].\end{aligned} \tag{7}$$

Combining Eqs. (1) and (7), the particle interference function is seen to be the sum of two terms:

$$\begin{aligned}P^{nn}_{(k)}=&\frac{1}{k}\int_{r=0}^{\infty}G^{V}_{(r)}H_{(r)}\sin(kr)dr\\&+\frac{1}{k}\int_{r=0}^{\infty}4\pi r\langle\rho\rangle^{V}\left[H_{(r)}+H'_{(r)}-\frac{\langle\rho\rangle}{\langle\rho\rangle^{V}}\right]\sin(kr)dr \ .\end{aligned} \tag{8}$$

By straightforward application of the convolution theorem of Fourier transform, the first term on the right-hand side can be expressed as a convolution integral, and the result for P^{nn} is[18]

$$P^{nn}_{(k)}=P^{V}_{(k)}\otimes W_{(k)}+S_{(k)} \tag{9}$$

with

$$W_{(k)}=\frac{1}{\pi}\int_{r=0}^{\infty}H_{(r)}\cos(kr)dr \tag{10}$$

and

$$S_{(k)}=4\pi\langle\rho\rangle^{V}\int_{r=0}^{\infty}r^2\left[H_{(r)}+H'_{(r)}-\frac{\langle\rho\rangle}{\langle\rho\rangle^{V}}\right]\frac{\sin(kr)}{kr}dr \ . \tag{11}$$

That is, the first term on the right-hand side of the expression for the interference function, Eq. (9), is the wide-angle scattering of the extended lattice, $P^{V}_{(k)}$, convoluted with the cosine transform of the intragrain correlation function. If size is the only cause of peak broadening, then $W_{(k)}$ gives the functional form of the profile of each Bragg reflection.

As a result of the subtraction of $\langle\rho\rangle$ in Eq. (3), there is no forward scattering in $P^{V}_{(k)}$.[23] Hence, the first term on the right-hand side in Eq. (9) does not contribute to small-angle scattering. On the other hand, the second term in (9) is the sine transform of the sum of functions without atomic-scale structure. Therefore, this term does not contribute to the interference function in the wide-angle region of a scattering pattern. Instead, this term describes the small-angle scattering of the array of particles.[24]

C. Nonreconstructed nanocrystal versus isolated particles

Since $W_{(k)}$ depends only on the intragrain correlation function, Eq. (9) has the important consequence that the wide-angle interference function is independent of the relative positions of the particles or grains. Therefore, if the lattice orientations are distributed at random, the wide-angle interference functions are identical for an array of isolated particles on the one hand and for a dense-packed arrangement of crystal grains in a polycrystal on the other. Note that the total atomic distribution function of a nanocrystalline solid contains a distribution (the intergrain contribution $\langle\rho\rangle^{V}H'_{(r)}$) of nonlattice interatomic spacings which, similar to the one of a gas, has no atomic-scale structure. In contrast to what intuition might suggest, this broad distribution does not imply a diffuse background in the interference function. Instead, the considerations above demonstrate that the interference function of a nonreconstructed nanocrystal differs from the one of a coarse-grained polycrystal by the size-induced peak broadening alone. This conclusion is in agreement with the notion of the absence of intergrain interference in polycrystals, i.e., of independent scattering of the individual crystal grains, involved in the derivation of formalism for Peak profile analysis,[28,34] and explicitly derived in Ref. 29. Since the difference between isolated particles, on the one hand, and a dense-packed polycrystalline aggregate on the other is only visible in small-angle scattering, experimental atomic distribution functions (in general determined from wide-angle scattering alone) cannot distinguish between the presence or absence of a "gaslike" intergrain contribution to the atomic distribution function.

It is noted that the absence of interference from the intergrain part of the atomic distribution function is a result of the fact that the interference function of a poly-

crystal is the average over a large number of grain boundaries with different lattice misorientations and grain-boundary plane orientations. Contrary to the polycrystal case, well-defined interference maxima arise in the scattering pattern of a bicrystal, that is in the case where the scattering volume contains only one single grain boundary.[30–32] In the average over many different boundaries, the amplitudes of the interference maxima of the individual boundaries add up to zero, therefore the scattering intensity vanishes.

It is instructive to consider the small-angle scattering for the limiting cases of a very dilute array of isolated particles and of a dense-packed, polycrystalline arrangement of grains. In the first case, with $H'_{(r)}=0$ and $\langle\rho\rangle=0$, Eqs. (11) and (9) combine to the familiar equation for small-angle scattering of an array of isolated particles.[25] In the second case, if the geometrical objects defining the external shape of the grains completely fill space, then, as the probability that a random vector originating at a random origin ends either inside the grain containing the origin or in one of the remaining grains is unity, it follows that $H_{(r)}+H'_{(r)}=1$. With $\langle\rho\rangle=\langle\rho\rangle^V$, the small-angle scattering interference function [Eqs. (11) and (9)] is seen to vanish identically.

D. Analysis of grain size distribution

The formalism which has been outlined above is a generalization of a similar formalism derived with the aim of determining the crystallite size distribution from scattering data.[18] Based upon the analogon to expression (9) for a set of geometrically similar particles or grains with a distribution of sizes, size distribution, and root-mean-square lattice strain are obtained from experimental scattering data by an indirect deconvolution of the Bragg reflection profiles, similar to a technique used in the analysis of small-angle scattering data.[33] The validity of area- and volume-weighted average grain sizes determined from those size distributions has been confirmed[17,18] by comparison with results from Warren-Averbach analysis[34] and from TEM histograms. The samples and scattering data considered in Ref. 18 are part of those at the present work. Area-weighted average grain sizes considered in the experimental part below were obtained by the indirect deconvolution method.

E. Nanocrystal with a disordered grain-boundary component

In a real polycrystal, the atomic structure in the grain-boundary region will be reconstructed, that is atoms will be displaced from their lattice positions to new, nonlattice equilibrium positions. The distribution of the interatomic spacings involving these positions may display preferred distances, that is there may be short-range order. On the other hand, it is conceivable that there is a large number of different local atomic structures, corresponding to different orientations of the neighboring crystal lattices and of the grain-boundary planes, and that on average over all those configurations there is little atomic short-range order. A simplistic description of this structure considers a grain-boundary layer in which the atomic positions are completely random. For simplicity, it is assumed that the atomic density in the grain-boundary layer is identical to the one in the crystallites, $\langle\rho\rangle^V$.

The atomic distribution function of this "disordered nanocrystal model" contains contributions from central atoms in the crystal grains and from central atoms in the boundary layer. For the central atoms in the crystal grains, the intragrain part of the atomic distribution function is $\rho^V_{(r)}H_{(r)}$, and since the atoms surrounding each crystal grain (layer plus remaining crystal grains) are arranged at random, with density $\langle\rho\rangle^V$, the remaining distances contribute $\langle\rho\rangle^V(1-H_{(r)})$ (compare Sec. II C). As the layer atoms are located randomly, the position of each of them is not correlated to the positions of the remaining layer atoms nor to those of the crystallite atoms. Therefore, the atomic distribution function of the layer atoms is a constant, $\langle\rho\rangle^V$. The total atomic distribution function of the disordered nanocrystal, $\rho^{\rm dn}_{(r)}$ is the sum of crystallite and layer atomic distribution functions, weighted by the fractions of atoms in the respective phases, which is

$$\rho^{\rm dn}_{(r)}=x_L H_{(r)}\rho^V_{(r)}+(1-x_L H_{(r)})\langle\rho\rangle^V , \tag{12}$$

where x_L denotes the fraction of atoms on crystal lattice sites (the ratio of the crystal site atoms over the total number of atoms in the solid). The reduced atomic distribution function has the simple form

$$G^{\rm dn}_{(r)}=x_L H_{(r)}G^V_{(r)} \tag{13}$$

and the interference function is

$$P^{\rm dn}_{(k)}=x_L P^V_{(k)}\otimes W_{(k)} \tag{14}$$

with $W(k)$ given by Eq. (10).

Equation (14) implies the interference function of the disordered grain-boundary layer model to be identical to the one of the nonreconstructed nanocrystal and of isolated crystalline particles, except for multiplication with a constant less than unity, the fraction of atoms in the crystalline particles. As a result, $P^{\rm dn}_{(k)}=-x_L$ in between Bragg peaks, where $P^V_{(k)}=-1$ [compare Eq. (4) and Sec. II A], which results in a diffuse background intensity

$$I^{\rm dn,diffuse}_{(k)}=V\langle\rho\rangle ff^*(1-x_L) . \tag{15}$$

If there is short-range order, as opposed to complete randomness, in the grain-boundary layer, then the layer contribution to the atomic distribution function is modulated on an atomic scale, and consequently the scattering intensity between the Bragg reflections is not a constant, but oscillates as a function of k. If the atomic density in the disordered layer is different from the one in the crystallites, then the small-angle scattering intensity will not vanish [as it does in Eq. (14)]; on the other hand, the wide-angle part of the scattering pattern will not be affected, and hence an experimental atomic distribution function determined from wide-angle scattering alone will be identical to the one obtained for the dense grain-boundary layer. In summary, the considerations in this section show that it is only in the case where a significant fraction of atoms are located on nonlattice sites that th wide-angle scattering by polycrystals with a random di

tribution of lattice orientations differs from the one of a set of isolated particles with the same size and shape as the grains in the polycrystal.

These results suggest two alternative ways to obtain quantitative information on the atomic short-range order (SRO) in the grain boundaries, characterized by the quantity x_L. First, x_L can be determined from the diffuse scattering intensity between the Bragg reflections. However, it is noted that the diffuse background may be hard to detect in experimental diffraction data: only when the nanocrystal is very fine grained will there be a significant fraction of grain-boundary atoms (their number scales with the total grain-boundary area). However, since the profile of the Bragg reflections widens when the grain size is reduced, there will also be appreciable overlap of the tails of the reflections in the fine-grained case. As the functional form of the reflection tails depend upon *a priori* unknown details of the distribution of crystal size and shape, as well as lattice strain, it will be problematic to distinguish the reflection tail contribution from the diffuse background indicative of nonlattice atoms at the grain boundaries. It is therefore preferable to characterize the grain-boundary SRO on the basis of the atomic distribution function. According to Eq. (12) that part of the atomic distribution function which displays SRO is $x_L H_{(r)} \rho^V_{(r)}$. As $\rho^V_{(r)}$ is known, the coefficient x_L can be determined from experimental atomic distribution functions. To do so, the relative reduction in coordination number, that is the ratio of the experimental number of atoms in the respective coordination shell in the nanocrystalline material, Z, over the coordination number of the ideal crystal lattice, Z^{ideal}, is plotted versus the interatomic distance, and the function $x_L H_{(r)}$ is determined as the straight line of best fit to this data. As $H_{(0)}=1$ [compare Eq. (6)], the value of the fit function at $r=0$ corresponds to the fraction of atoms on crystal lattice sites, x_L. This analysis will be applied to experimental data in Sec. V below.

III. PREPARATION, X-RAY SCATTERING, AND DATA ANALYSIS

Samples of nanocrystalline Pd were prepared by the inert gas condensation method, described in detail in Refs. 35 and 36. The inert-gas condensed Pd powder was consolidated *in situ* under high vacuum. This consolidation was achieved at room temperature during a 5 (10) min time interval at a pressue of 1 (2) GPa for a first (second) set of samples; it yields samples with a density, as determined by Archimedes' immersion method, of typically 84% (87%) of the coarse-grained Pd literature value. Samples prepared in this way will be designated "RT consolidated." Some samples underwent an additional, *ex situ* 48–72 h densification step at 100 °C and 3.2 GPa, which increased the density to about 93–96 %; samples in this state will be designated as "warm consolidated." The samples are disk-shaped with a diameter of 8 mm and a thickness of 100–300 μm. No metallic impurities were detected in a scanning microprobe. Hot extraction on four samples yielded 0.6±0.2 at. % O, 0.3±0.1 at. % N, 0.4±0.3 at. % H.

Annealing at various temperatures was performed, at a vacuum of $<10^{-6}$ mbar, in an externally heated silica tube furnace connected to a turbomolecular pump. Individual anneals were for 24 h.

X-ray scattering data were recorded by a Siemens D-5000 θ-θ diffractometer with Mo $K\alpha$ radiation monochromatized by a Si(Li) solid-state detector. The instruments θ-dependent, variable aperture slit system achieves a constant irradiated sample area (6.6* 4 mm^2). The angular variation of the primary beam intensity due to the variable aperture was experimentally determined and corrected for during data evaluation. The intensity was recorded in the angular range 5°–155° at intervals of 0.01°, with a total scan time of 90 h per sample. Standard procedures[37,38] were used to correct for the atomic form factor, for polarization, absorption and for wave-vector-dependent discrimination of incoherent (Compton) scattering (see details in Ref. 39). Air scattering was negligibly small (a maximum of 4% of the total intensity at $2\theta=5°$, and less than 1.5% for $2\theta>10°$) at all angles. The scattering intensity was normalized to absolute units using the condition that the computed interference function must satisfy the relation [the limiting case of Eq. (2) for $r \ll 1/k_{\max}$ (Ref. 39)]

$$-2\pi^2\rho_0 \approx \int_0^{k_{\max}} k^2 P_{(k)} dk \ . \tag{16}$$

The function $G_{(r)}$ was determined from the corrected data by evaluating the integral in Eq. (2), with a linear extrapolation to zero for the interference function at $k<0.77$ Å^{-1}, and a maximum wave vector $k_{\max}=17.3$ Å^{-1}. No artificial damping function was used.

A value for the average density $\langle\rho\rangle$, required in order to consistently determine $\rho_{(r)}$ from $G_{(r)}$ [compare Eq. (3)], was obtained from the variation of $G_{(r)}$ in the region between the origin and the first nearest-neighbor spacing, where $G_{(r)}$ oscillates around $-4\pi r\langle\rho\rangle$. In this region, $G_{(r)}$ is sensitive to small errors in data correction, and consequently the value for $\langle\rho\rangle$ could be determined with an accuracy limited to about ±5%. The result of an incorrect choice of $\langle\rho\rangle$ is readily seen [compare Eq. (3)] to be the erroneous addition of a constant background to $\rho_{(r)}$. The resulting uncertainty in the background between the crystalline coordination shell peaks in the experimental atomic distribution function is therefore ±5% of $\langle\rho\rangle$.

IV. ANALYSIS OF THE ATOMIC DISTRIBUTION FUNCTIONS

Our primary interest in analyzing the experimental atomic distribution functions was to determine the coordination numbers Z of the individual coordination shells of the Pd crystal lattice. These quantities have been related, in Sec. II E, to the atomic SRO of the grain boundaries. Coordination numbers were determined by fitting sets of Gaussians to the experimental $\rho_{(r)}$. If the contribution of a peak "j" to $\rho_{(r)}$ is given by

$$\rho_{j(r)} = \frac{a_j}{\sqrt{2\pi}\sigma_{\text{expt},j}} \exp - \frac{(r-r_j)^2}{2\sigma^2_{\text{expt},j}} \tag{17}$$

then the coordination number is obtained, by integrating the function $4\pi r^2\rho_{(r)}$, as[39]

$$Z_j = 4\pi a_j(\sigma^2_{\text{expt},j} + r_j^2) \ . \tag{18}$$

In addition to the coordination numbers, it is of interest to characterize the width of the distribution of interatomic spacings, which is a measure for the atomic SRO in the crystal lattice. Displacements of atoms from the ideal lattice sites may be dynamic and related to the phonon spectrum of the material, or else they may be static and related to the defect structure. In order to determine the distribution of the interatomic spacings in nanocrystalline Pd, it is necessary to discuss how the atomic displacements are represented in the "true" atomic distribution function, and how the "true" function relates to the one determined experimentally.

The consequences of the atomic displacements on the atomic distribution function are treated in Ref. 40. Let the atoms be displaced at random from their crystalline lattice sites, with the probability $c_{(x,y,z)}$ of finding an atom displaced by the vector (x,y,z) given by the normalized, three-dimensional Gaussian of variance σ_{disp}:

$$c_{(x,y,z)} = \frac{\exp(-x^2/2\sigma^2_{\text{disp}})\exp(-y^2/2\sigma^2_{\text{disp}})\exp(-z^2/2\sigma^2_{\text{disp}})}{(2\pi\sigma^2_{\text{disp}})^{3/2}} \ . \tag{19}$$

Then the distribution of interatomic spacings in $G_{(r)}$ is also a Gaussian. As the distribution of interatomic spacings involves displacements of both the central atom and its neighbors, the variance of the distribution of spacings in the atomic distribution function, σ_{ADF}, is larger than that relating to the displacement of the individual atoms: $\sigma^2_{\text{ADF}} = 2\sigma^2_{\text{disp}}$ provided that the atomic positions are crystallographically equivalent and that the individual displacements are independent.[40] If the distribution of interatomic spacings in the jth shell was a δ function at r_j, then the contribution of that shell to the reduced interference function $F_{(k)} = kP_{(k)}$ is a sine wave $F^0_{j(k)} = Z_j r_j^{-1}\sin(kr_j)$. For the Gaussian distribution of spacings, the sine wave is multiplied by $\exp(-\sigma^2_{\text{ADF},j}k^2/2)$.[40] If the distributions of interatomic spacings in all the coordination shells had the same variance, then this factor was identical to the Debye-Waller factor of the crystal lattice, $\exp(-\langle u_x^2\rangle k^2)$,[41] where $\langle u_x^2\rangle$ is the mean square of the projection of the atomic displacements on the x axis,[42] and $\langle u_x^2\rangle = \sigma^2_{\text{disp}}$.

In order to determine the "true" atomic distribution function from experimental scattering data, one has to measure the interference function in the k interval where it displays significant structure, that is to a maximum wave vector considerably larger than $2/\sigma_{\text{ADF}}$. With laboratory x-ray sources, the accessible $k_{\max}$ is generally such that this condition is not satisfied. As a result of the truncation of the interference function at $k_{\max}$, the contribution of shell "j" to the experimental atomic distribution function is not a Gaussian, but a function displaying spurious oscillations on both sides of a broadened central peak. The experimental reduced atomic distribution function of shell "j," $G^{\text{expt}}_{j(r)}$, is given by

$$G^{\text{expt}}_{j(r)} = \frac{2}{\pi}\int_0^\infty F^0_{j(k)}V_{j(k)}\sin(kr)dk \tag{20}$$

with $V_{j(k)} = \exp(-\sigma^2_{\text{ADF},j}k^2/2)$ for $k \le k_{\max}$, and $V_{j(k)} = 0$ for $k > k_{\max}$. Applying the convolution theorem of Fourier transform, and the relation between $G_{(r)}$ and $\rho_{(r)}$, Eq. (3), the corresponding contribution to the experimental atomic distribution function is found to be

$$\rho^{\text{expt}}_{j(r)} = \frac{Z_j}{4\pi^2 r_j}\frac{1}{r}\int_0^{k_{\max}} \exp\left[-\frac{\sigma^2_{\text{ADF},j}k^2}{2}\right] \times\cos[k(r-r_j)]dk \tag{21}$$

which yields the Gaussian shape of the "true" atomic distribution function only in the limit $k_{\max,j} \gg 2/\sigma_{\text{ADF},j}$. For smaller $k_{\max}$, the integral has no analytic solution.

In the present work, the diffraction data were recorded with Mo $K\alpha 1/2$ radiation. Hence, the data are a superposition of two interference functions recorded with different wavelengths, those of the $K\alpha 1$ and $K\alpha 2$ lines. Consequently, the peaks in the experimental atomic distribution function are also the superposition of two peaks

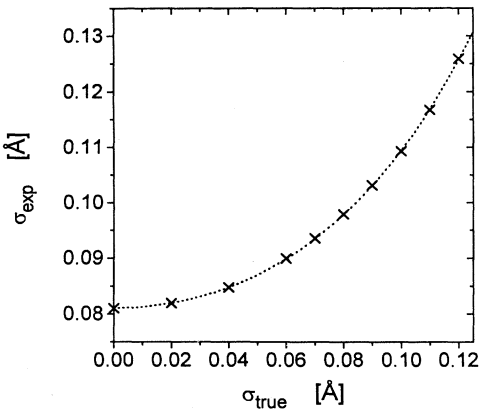

FIG. 3. Variance σ_{expt} of the nearest-neighbor peak in the atomic distribution function as determined from a fit of Gaussians to the numerically simulated experimental peak shape vs "true" coordination shell variance σ_{ADF} for a Mo $K\alpha 2/2$ radiation experiment with a maximum experimental wave vector $k_{\max} = 17.3$ Å^{-1}. The dotted line is an empirical fit to the data by the relation indicated in the text.

of the form given by Eq. (21), ρ_{j1} and ρ_{j2}, centered at $r_{j1}=r_j\langle\lambda\rangle/\lambda_1$ and $r_{j2}=r_j\langle\lambda\rangle/\lambda_2$, respectively. λ_1, λ_2, and $\langle\lambda\rangle$ are the wavelengths of Mo $K\alpha 1$, $K\alpha 2$, and their weighted average, respectively. The peak in the experimental atomic distribution function has the form $\rho_{j(r)}^{\text{expt},K\alpha 1/2}=(\rho_{j1(r)}+Q\rho_{j2(r)})/(1+Q)$, with Q the intensity ratio of the two wavelengths.

In order to relate the experimental variance of the first nearest neighbor peak of Pd at $r_1=2.75$ Å, determined by fitting Gaussians to the experimental atomic distribution function, to the "true" variance, we calculated $\rho_{j(r)}^{\text{expt},K\alpha 1/2}$ numerically for a number of "true" variances, and for $k_{\max}=17.3$ Å^{-1}. The resulting numerical solutions were fitted by Gaussians. The relation between σ_{ADF} and σ_{expt} obtained in this way is displayed in Fig. 3. In the interval of interest, the data are interpolated by the empirical function

$$\sigma_{\text{expt}}=0.0811\ \text{Å}+2.23\ \text{Å}^{-1}\sigma_{\text{ADF}}^2+60.5\ \text{Å}^{-3}\sigma_{\text{ADF}}^4 .$$

This relation is used below to determine the "true" variance of the distribution of interatomic spacings in nanocrystalline Pd from the variance of the Gaussian of best fit to the experimental atomic distribution functions. A comparison of the experimental atomic distribution function of nanocrystalline Pd to the peak shapes obtained in this way and to that of the Gaussian of best fit is given in Fig. 11 in Sec. V B.

V. EXPERIMENTAL RESULTS AND DISCUSSION

A. Grain size, strain, and density

A total of 18 wide-angle x-ray scattering data sets were recorded. Of those, 2 were for coarse-grained reference

TABLE I. Macroscopic sample density and comparative listing of different measures for grain size and lattice strain: full width at half maximum (FWHM) based average grain size $\langle D\rangle_{\text{FWHM}}$ and e_{FWHM} (determined in the $\langle 111\rangle$ direction according to Ref. 44); area- and volume-weighted grain size $\langle D\rangle_{\text{area}}$, $\langle D\rangle_{\text{volume}}$ and strain $\langle\varepsilon^2\rangle^{1/2}$ (determined in the $\langle 111\rangle$ direction according to Ref. 18). The far left column designates the sample and the treatment it underwent between the respective investigation and the previous one. Densities denoted "n.d." in the table were not determined.

	$\langle D\rangle_{\text{volume}}$ (nm)	$\langle D\rangle_{\text{area}}$ (nm)	$\langle\varepsilon^2\rangle^{1/2}$ (%)	$\langle D\rangle_{\text{FWHM}}$ (nm)	e_{FWHM} (%)	ρ_{geo} (%)
Pd01, aged	35	18	0.026	35	0.056	85
Pd01, annealed 100 °C	56	23	0.001	55	0.030	87
Pd01, warm compacted	63	34	0.081	76	0.132	93
Pd01, annealed 160 °C	68	39	0.060	76	0.093	94
Pd01, annealed 300 °C	81	69	0.028	85	0.067	n.d.
Pd02, aged	25	16	0.070	24	0.140	83
Pd02, annealed 100 °C	42	22	0.015	44	0.048	86
Pd02, warm compacted	32	23	0.107	37	0.188	93
Pd02, annealed 160 °C	39	26	0.031	38	0.076	94
Pd05, aged, warm compacted	40	23	0.103	37	0.137	94
Pd06, aged	31	19	0.108	29	0.126	84
Pd07, aged, warm compacted	17	11	0.155	18	0.277	93
Pd03, as prepared, warm compacted	20	13	0.089	21	0.146	94
Pd03, annealed 160 °C	35	15	0.052	36	0.085	n.d.
Pd04, as prepared	24	11	0.093	26	0.206	87
Pd04, annealed 100 °C	63	17	0.019	80	0.038	n.d.

samples (commerical polycrystalline powder and 700 °C vacuum-annealed nanocrystalline sample Pd01). The remaining data were recorded on 7 nanocrystalline samples at various age and after different thermal and mechanical treatments.

For samples Pd01, Pd02, Pd05, Pd06, Pd07 the first scattering data with a quality sufficient for quantitative analysis were recorded about 4 months after preparation. The state of these samples will be referred to as "aged." Shorter x-ray scans recorded during this interval evidence significant room-temperature grain growth,[43] more than doubling the average grain size as determined by the method described in Ref. 44, assuming Gaussian strain and Cauchy size broadening, and a decrease in the root-mean-square (rms) lattice strain. For samples Pd03 and Pd04, the first high-quality x-ray data were recorded within 10 days of the preparation; we shall designate this state "as prepared."

Table I lists the density, as well as the area and volume-weighted averages of the grain-size $\langle D \rangle_{\text{area}}$ and $\langle D \rangle_{\text{volume}}$, and the rms strain $\langle \varepsilon^2 \rangle^{1/2}$ as determined by the indirect deconvolution method (see Ref. 18 and Sec. II D), and from the Bragg peak FWHM, assuming Gaussian strain and Cauchy size broadening.[44] It is seen that the lattice strain is highest in the warm-consolidated samples, and that the as-prepared samples have the smallest grain size.

B. Atomic distribution functions

1. General

For the example of nanocrystalline sample Pd02 in the aged state, Fig. 4 displays the various functions involved in the data evaluation procedure: scattering intensity, interference function, reduced interference function $kP_{(k)}$,

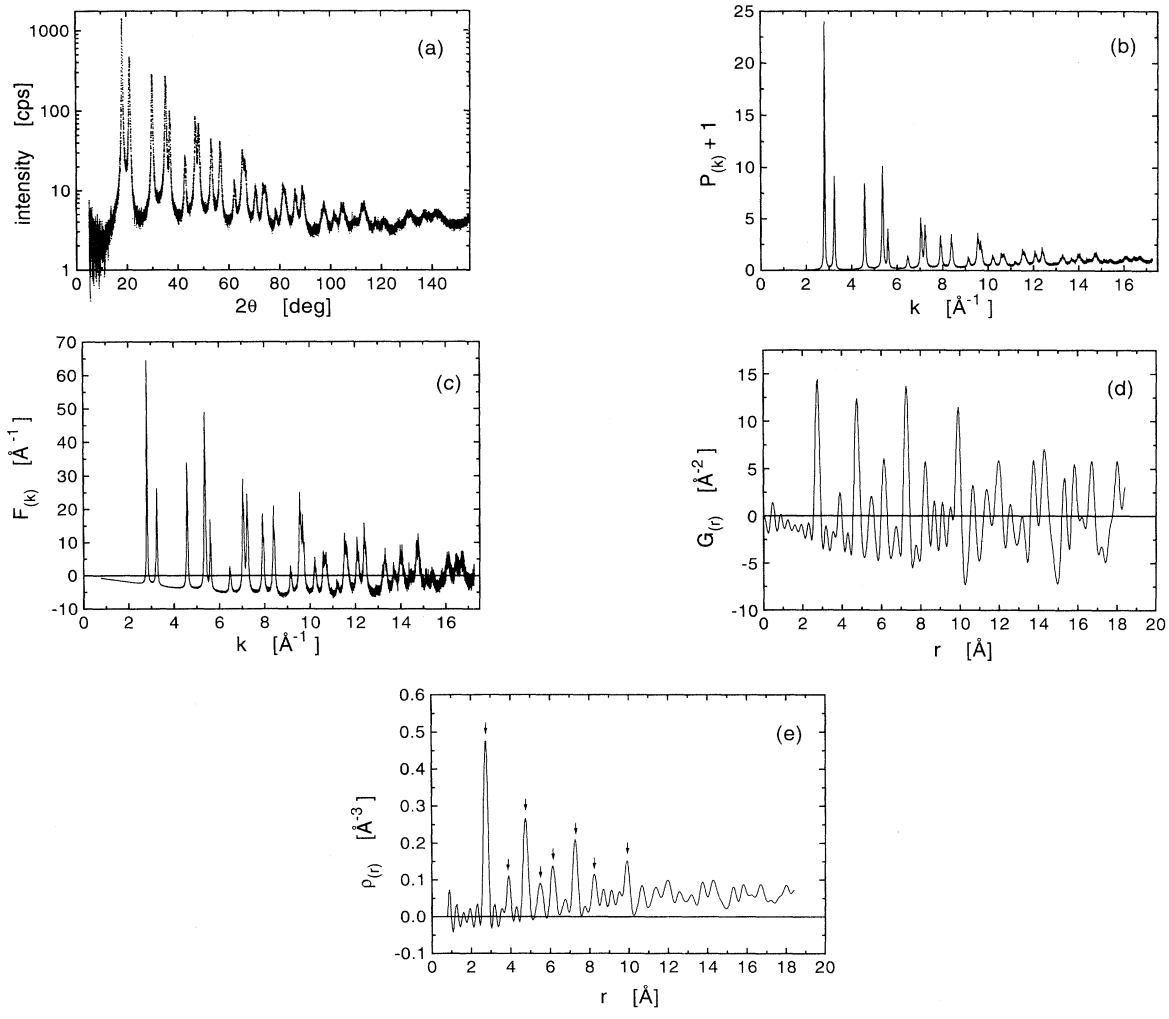

FIG. 4. Functions involved in the x-ray data evaluation, for the example nanocrystalline sample Pd02, aged 4 months at room temperature: (a) scattering intensity I vs scattering angle 2Θ; (b) interference function $P+1$ vs wave vector k; (c) reduced interference function $F=kP$ vs k; (d) reduced atomic distribution function G vs interatomic spacing r; (e) atomic distribution function ρ vs r. Arrows in (e) denote those coordination shells which were used in the analysis of the coordination number (compare Fig. 6).

reduced atomic distribution, and atomic distribution function. Two more examples for interference and atomic distribution functions are depicted in Fig. 5, one for Pd03 as-prepared, and one for the coarse-grained powder reference sample. In Fig. 4(e), the eight strongest peaks in $\rho_{(r)}$, considered in the analysis of the coordination numbers below, are designated by arrows. The spurious oscillations between the coordination peaks displace when the upper limit of the integration in Eq. (2) is varied. Hence, these oscillations are not related to atomic structural features in the "true" atomic distribution functions of the samples. Instead, they are artifacts due to the truncation of the interference function at 17.3 $Å^{-1}$, and due to experimental errors in the data reduction (compare also Secs. IV and V B 3). The small amplitude of the oscillations at small r indicates a successful data reduction.

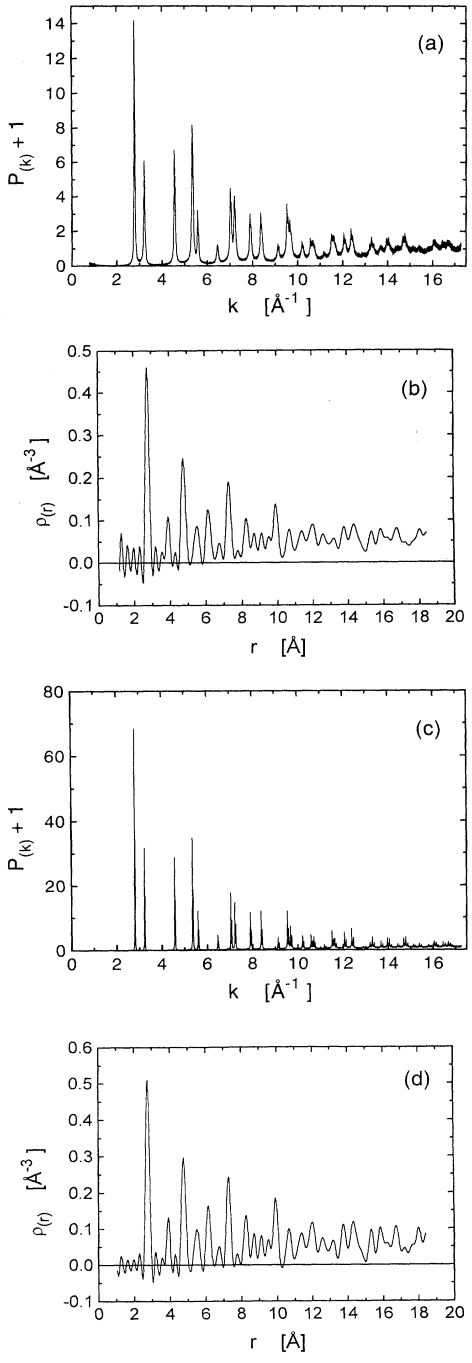

FIG. 5. Interference and atomic distribution functions for sample Pd03 warm-consolidated, as-prepared (a) and (b) and for coarse-grained powder reference sample (c) and (d).

The atomic distribution functions are seen to exhibit sharp coordination shell peaks; no significant background indicative of a disordered grain-boundary component is detected. Qualitatively similar atomic distribution functions were obtained for the reference samples and for all nanocrystalline samples, independent of age or thermal and mechanical treatment.

2. *Coordination numbers*

In order to compare the experimental atomic distribution functions to the predicted ones derived for the different models of grain boundary structure (Sec. II E), the coordination numbers of the eight strongest peaks in the atomic distribution function were determined from fits of Gaussian functions to the experimental atomic distribution function (see Sec. IV).

The ratio of the experimental coordination numbers, Z_j, over the coordination number of the ideal, infinite fcc lattice, Z_j^{ideal}, corresponds to the product of the intragrain correlation function H at interatomic distance r_j and the fraction of atoms on crystal lattice sites x_L [compare Eq. (12)]. As H should be a linear function at small r [compare Eq. (6)], the function $x_L H_{(r)}$ was determined as the straight line of least-squares deviation to the ratios Z_j/Z_j^{ideal}, that is to the relative coordination numbers at interatomic distance r_j. Figure 6 shows examples for this type of plot for reference and nanocrystalline samples. Errors in Z arise from the spurious oscillations in the experimental atomic distribution functions (compare Sec. V B 1). The error bars in the figure correspond to the area under one such oscillation, their dependence on r arises from the empirical finding that the amplitude of the oscillations in the function $G_{(r)}$ is nearly independent of r. The absolute error, ΔZ, increases with the interatomic distance; however, the relative error, $\Delta(Z/Z^{\text{ideal}})$, is largest for the coordination shell with the smallest Z^{ideal}, that is the second-nearest-neighbor shell at 3.95 Å.

As can be seen in Fig. 6, the relative coordination numbers are on average less than unity, and diminish with increasing interatomic distance. This implies that the coordination numbers on crystalline coordination shells in nanocrystalline Pd are smaller than those in coarse-grained Pd samples. For all samples, the relative coordination numbers decrease linearly with r within error bars. This agrees with the predictions, in Sec. II, for the decrease in coordination number due to the size effect in isolated particles and nanocrystals. The coordination numbers of the two coarse-grained samples diminish slightly with increasing interatomic distance. This is due

to the instrumental broadening of the Bragg reflections. The experimental interference function is the convolution of the true interference function with the instrumental resolution function. The effect of the instrumental broadening on the atomic distribution function is therefore similar to the effect of grain-size-induced broadening, that is the multiplication with a function which diminishes with increasing interatomic distance. The resulting reduction of the coordination numbers in the higher-order coordination shells of the coarse-grained samples is seen to be considerably smaller than the reduction in the nanocrystalline samples.

Figure 7 depicts the specific grain boundary area as determined by two different methods. The quantity $\alpha_{GB,ADF}$ is inferred from the slope of the straight line of best fit to the relative coordination numbers [compare Eq. (6)]; in order to correct for the instrumental effects mentioned above, the slope of the fit for the coarse-grained reference powder was subtracted in each case. The quantity $\alpha_{GB,D}$ is determined from the area-weighted average grain size, determined by the indirect deconvolution method:[18] $\alpha_{GB,D}=3/\langle D\rangle_{area}$. As other evidence (see below) suggests that the fit function for samples Pd03 and Pd04 in the as-prepared state must not be identified with the intragrain correlation function of the crystallites, the corresponding results are not included in the diagram. It is seen that most data points lie, within error bars, on a straight line through the origin, with slope unity. This correlation indicates that for the samples listed in the figure, the observed reduction in coordination number can be attributed to the particle size effect, described by Eqs. (5) and (6). The quantitative agreement of the reduction deduced from the atomic distribution functions with the one predicted from the specific grain-boundary area evidences that grain boundaries as opposed to free surfaces of pores in the 84–96 % dense samples are responsible for the reduced coordination number.

As indicated above, the value at $r=0$ of the straight line of best fit to the relative coordination numbers represents the fraction of atoms on crystal lattice sites. Figure 8 depicts the value of x_L obtained in this way as a function of the specific grain-boundary area $\alpha_{GB,D}$. The squares refer to the reference samples and to all samples aged at RT for at least 4 months or annealed. The crosses refer to samples Pd03 and Pd04 investigated within 10 days after preparation. For the first set of samples, the average value of x_L is 0.99. Within error bars of about 4%, x_L is seen to be unity. This confirms the validity of Eqs. (5) and (6) for the aged and annealed samples, and implies that, within error bars, all atoms are located on lattice sites. On the other hand, for the as-prepared samples (aged for less than 10 days), x_L is significantly less than unity. This indicates that for the as-prepared samples a significant fraction of atoms (8 and 14 %) are not located on lattice sites. After annealing to 160 °C (Pd03) and 100 °C (Pd04), the parameters x_L for those

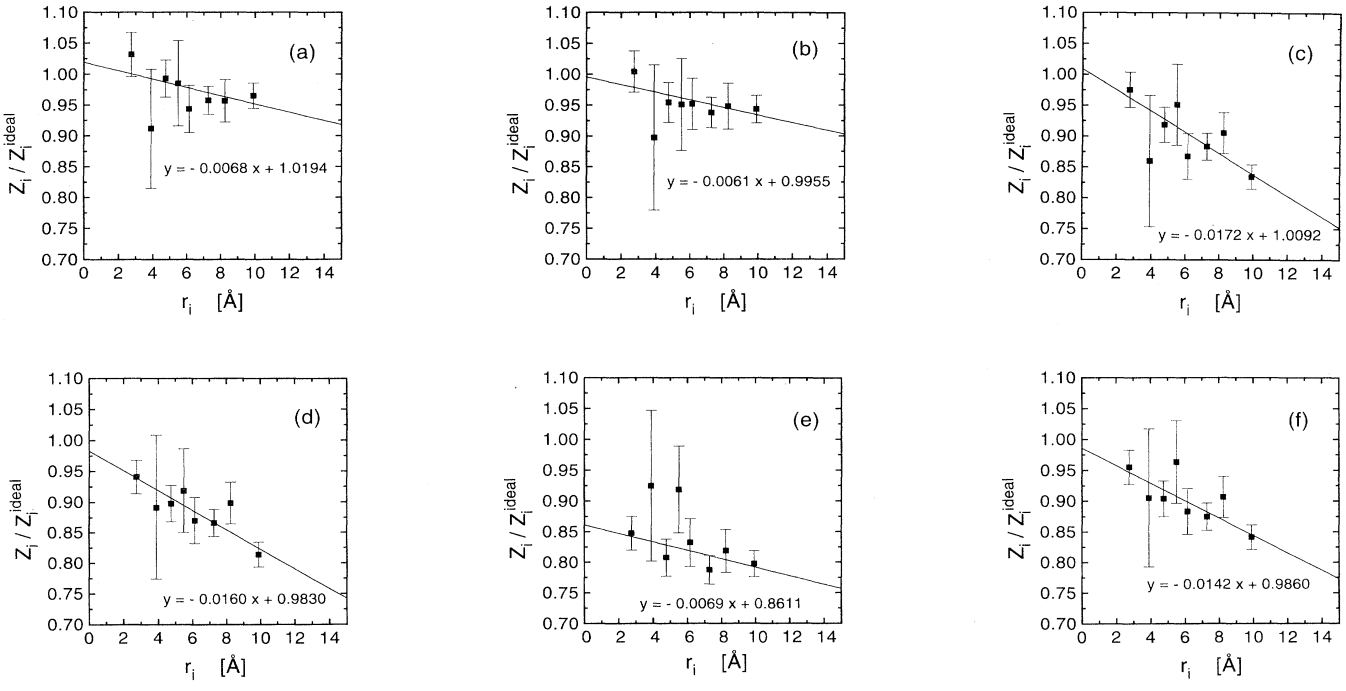

FIG. 6. Ratio Z_i/Z_i^{ideal} of the experimental number of atoms in coordination shell i, Z_i, over the ideal single-crystal value for that shell, Z_i^{ideal} vs interatomic spacing r_i. (a) coarse-grained Pd powder reference; (b) reference Pd01 annealed at 700 °C; (c) Pd01 cold-consolidated, aged; (d) Pd01 annealed 100 °C; (e) Pd03 warm-consolidated, as-prepared; (f) Pd03, annealed 160 °C. Solid lines: $x_L H_{(r)}$ obtained by linear least-squares fit to the data; the numbers in the figures indicate the fit parameters.

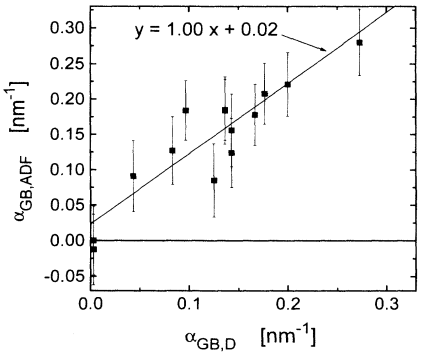

FIG. 7. The specific grain-boundary area $\alpha_{GB,ADF}$ determined from the atomic distribution function (vertical axis) vs the specific grain-boundary area $\alpha_{GB,D}$ from the grain size distribution determined by the indirect deconvolution technique (horizontal axis). The linear least-squares fit to the data in the figure (solid line) is close to a straight line through the origin.

two samples increased to 0.99 and 0.95, respectively, that is to values inside the range found for the aged or annealed samples. Figure 9 shows x_L as a function of sample age for cold-compacted and warm-compacted samples. Data from annealed samples are not shown in this figure. The data indicate that a change in atomic SRO takes place on a time scale of several weeks. Apart from this apparent influence of aging no other systematic correlation could be found between x_L and the preparation or annealing conditions.

Atoms on nonlattice sites have been considered in the model of the disordered grain-boundary layer, Sec. II E. In order to examine whether the data for the as-prepared samples match the reduced atomic distribution function

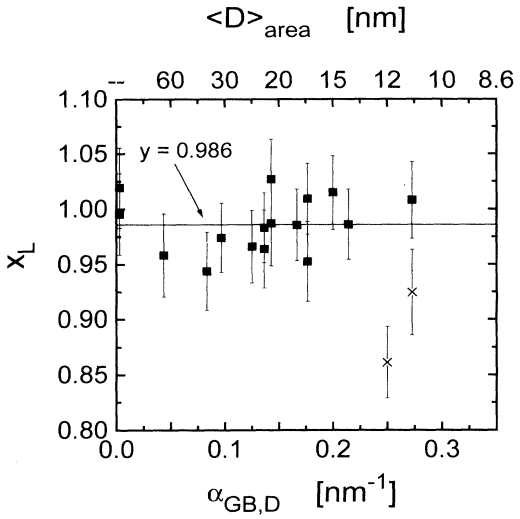

FIG. 8. Fraction of atoms on crystal lattice sites x_L as a function of the specific grain-boundary area $\alpha_{GB,D}$. The corresponding area-averaged grain size $\langle D \rangle_{area}$ is indicated on the top horizontal axis. Squares, samples aged for at least four months or annealed and reference samples; crosses, as-prepared samples, i.e., aged for less than 10 days. The solid line represents the average value of x_L for the aged, annealed, and reference groups of samples.

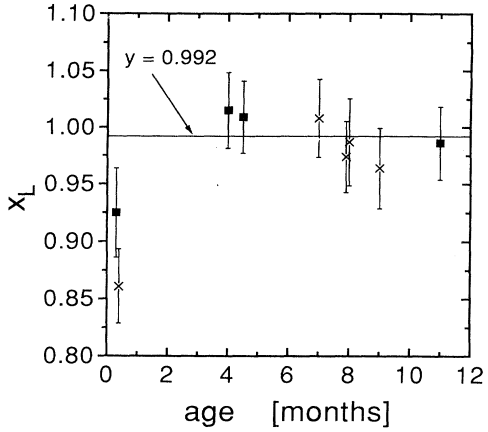

FIG. 9. Fraction of atoms on crystal lattice sites x_L as a function of aging time at room temperature for samples consolidated at room temperature (squares) and for warm-consolidated samples (crosses).

predicted by the disordered grain-boundary model, Eq. (13), the experimental reduced atomic distribution functions of the nanocrystalline samples, G^{nano}, are fitted by the expression

$$G^{nano}_{(r_j)} = x_L \left[1 - \frac{\alpha_S}{4} r_j\right] G^{ref}_{[(1+q)r_j]} , \quad 2.5 < r_j < 20 \text{ Å} \qquad (22)$$

with G^{ref} the experimental reduced atomic distribution function of the commerical coarse-grained powder, and with the fraction of atoms on lattice sites x_L, the specific surface area α_S, and the difference in lattice constant $q = \Delta a / a$ as adjustable parameters. The quality of the fit is illustrated in Fig. 10. The values of x_L obtained in this way agree well with those obtained from the fits to the coordination shells, see Table II. This confirms the finding that a significant fraction of atoms are not located on lattice sites for the as-prepared samples. As the atomic distribution function of those samples contains no other peaks except for the crystalline ones [see Fig. 5(b)], there appears to be very little atomic short-range order near the nonlattice atoms.

If the number of atoms on nonlattice positions per unit

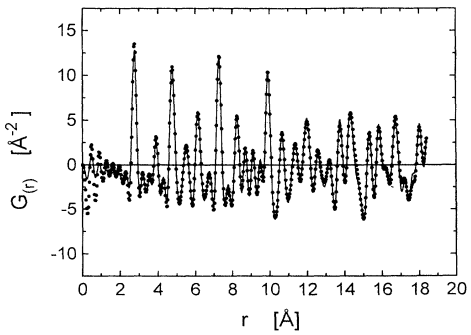

FIG. 10. Experimental reduced atomic distribution function (solid circles) for nanocrystalline sample Pd03 as prepared, and fit by Eq. (22) with coarse-grained Pd powder as the reference sample (solid line).

TABLE II. Comparative listing of the fraction of atoms on crystal lattice sites, x_L, determined by two alternative methods, for a number of samples.

Sample+state	x_L determined according to Eq. (22)	x_L determined according to Eq. (12)
Pd01, aged	1.00	1.01
Pd02, aged	0.99	1.01
Pd03, as prepared, warm compacted	0.86	0.86
Pd03, annealed 160 °C	0.96	0.99
Pd04, as prepared	0.93	0.92
Pd04, annealed 100 °C	0.95	0.95

area of grain boundary was the same for all samples, independent of grain size, then the fraction of nonlattice atoms would be proportional to the specific grain-boundary area. Hence, the fraction of lattice atoms, x_L, would be $x_L = 1 - \alpha_{GB} t$, with t the thickness of a hypothetical disordered GB layer of the same density as the crystal lattice. Fits of this relation to the data in Fig. 8, with t as the variable, yield $t = 0.06 \pm 0.05$ nm for the combined set of aged, annealed, and reference samples and $t = 0.41 \pm 0.09$ nm for the as-prepared samples. With a literature value of 68.0 nm^{-3} for the atomic density of Pd, this corresponds to 4 ± 3 atoms per nm^2 on nonlattice sites for the first-mentioned group and 28 ± 6 atoms/nm^2 on nonlattice sites for the second group. Another way to express the result is in terms of atomic monolayers: with 15.3 atoms/nm^2 in a dense-packed crystal plane of Pd corresponding to one monolayer, we obtain 0.26 ± 0.2 monolayers and 1.8 ± 0.4 monolayers of atoms on nonlattice sites at the grain boundaries. If the "grain-boundary region" was defined as the outer atomic monolayer in each of the two crystals adjacent to a grain boundary, then in the aged or annealed samples about 1/8 of the atoms in the grain-boundary region were located on nonlattice sites, whereas all the grain-boundary atoms were located on nonlattice sites in the as-prepared samples.

For the aged and annealed samples, since essentially all atoms are located on lattice sites, the model of the nonreconstructed grain boundary appears to be a reasonably good approximation. Therefore the intergrain part of the atomic distribution function, which accounts for the interatomic spacings across the grain boundary, that is for the atomic short-range order in the grain-boundary plane, should be comparable in magnitude to the intergrain part derived for the nonreconstructed grain-boundary model. This part of the atomic distribution function is given by the second term of the sum on the right-hand side of Eq. (5). For a grain size of 10 nm, its magnitude is estimated [making use of Eqs. (5) and (6) with $H'_{(r)} \approx 1 - H_{(r)}$ as discussed in Sec. II C] to be 4.5% of $\langle \rho \rangle$ at an interatomic distance of 3 Å, that is in between the first- and second-nearest-neighbor coordination shells, where a slowly varying background should be easiest to detect. The magnitude of the background arising from the intergrain part of ρ is therefore comparable to the experimental error in $\langle \rho \rangle$ (compare Sec. III). Hence, the background is below experimental resolution. However, if there was a short-range-order peak in this component of ρ, a peak should be observable in the experimental atomic distribution functions. The fact that no such peak is observed indicates that for the aged and annealed samples there is, on the average over all grain boundaries in a sample, no preferred interatomic distance between atoms separated by a grain-boundary plane.

In principle, the intergrain part of the atomic distribution function in the aged or annealed samples could peak at the same interatomic distance, r_{NN}, as the intragrain part. In other words, the distribution of the nearest-neighbor spacings crossing a grain-boundary plane could be similar to the distribution of the nearest-neighbor spacings in the crystal lattice. In this case, the experimental nearest-neighbor coordination number Z_1 would be systematically larger than predicted by Eqs. (5) and (6). However, Z_1 was found to vary in agreement with Eqs. (5) and (6) [compare Figs. 6(c)–6(f)], indicating that the intergrain part of ρ does not peak at r_{NN}. In addition, such a high degree of short-range order requires atomic reconstruction of the grain-boundary regions, displacing atoms from their ideal lattice positions and widening the distribution of interatomic spacings. The analysis of the distribution of interatomic spacings in the nearest-neighbor coordination shells (Sec. V B 3) evidences against this possibility.

In the case of the as-prepared samples, of the order of 10% of the atoms are located on nonlattice sites. If, on the average over all grain boundaries in a sample, there existed preferred interatomic spacings, then this would result in an observable variation in the experimental atomic distribution function of those samples, that is an additional, larger than error bar peak in the atomic distribution function should occur. The absence of such a peak [compare Fig. 5(b)] evidences that SRO (in the above sense, that is on the average over all boundaries) is weak or absent for the nonlattice component in the as-prepared samples. On the other hand, the results do not exclude the existence of a variety of different grain-boundary structures, each having its own, characteristic local atomic configuration.

3. *Distribution of lattice interatomic spacings*

It is of interest to examine whether a modification of the local order in the crystal lattice as a function of grain size can be detected in the atomic distribution functions. Displacements of atoms from the ideal lattice sites widen the distribution of interatomic spacings for the crystal lattice coordination shells, as discussed in Sec. IV. Figure 11 shows a fit of Gaussians to the first 4 coordination shells in the experimental atomic distribution function, for the example of sample Pd01 in the aged state. Also shown is the function $\rho_{j(r)}^{\text{expt},K\alpha 1/2}$ for the nearest-neighbor

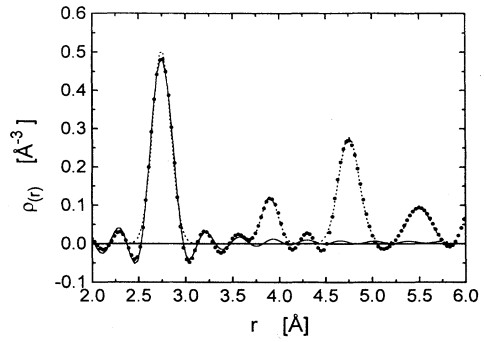

FIG. 11. Fit by Gaussians (dotted line) to the experimental atomic distribution function (solid circles). Sample Pd01, cold-consolidated, aged. The solid line is the experimental peak shape $\rho_{j(r)}^{\text{expt},K\alpha 1/2}$ (compare Sec. IV) corresponding to the Gaussian fit to the first-nearest-neighbor peak.

peak (compare Sec. IV), with the "true" variance σ_{ADF} determined from the variance of the Gaussian of best fit to that peak, σ_{expt}, via the empirical relation derived in Sec. IV and Fig. 3. The numerical model is seen to be in excellent agreement with the experimental data in the main peak, and to reproduce fairly accurately the position and the amplitude of the spurious oscillations. Similar fits to atomic distribution functions from reference and as-prepared samples are of identical quality. This indicates that the coordination shells in the "true" atomic distribution function of the samples are well approximated by Gaussians, and that their "true" variance is correctly determined from the empirical relation derived in Sec. IV.

Figure 12 displays the values of the experimental and true variances for the nearest-neighbor coordination shell as a function of the grain size. No systematic correlation

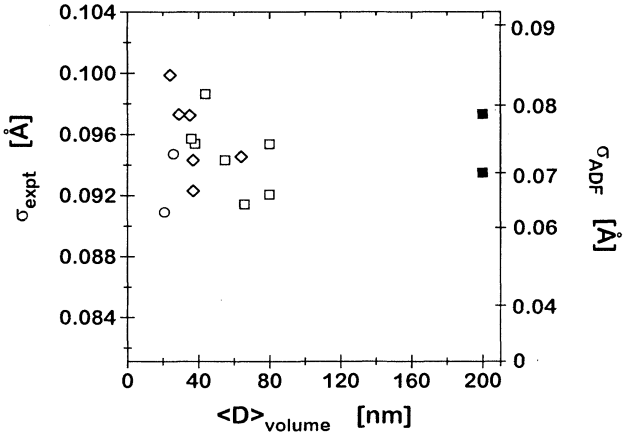

FIG. 12. Variance σ of the nearest-neighbor coordination shell peaks in the experimental atomic distribution functions plotted vs grain size $\langle D \rangle_{\text{volume}}$. Solid squares, reference samples; open circles, as-prepared samples; open diamonds, aged samples; open squares, annealed samples.

between variance and grain size is found. As in the case of the value x_L, there is also no measurable systematic correlation of σ to the preparation or annealing conditions. The data indicate identical "true" variances of 0.074±0.005 Å and 0.074±0.01 Å for reference and nanocrystalline samples, respectively, corresponding to about 2.7% of the nearest-neighbor interatomic spacing. Within error bars the distribution of interatomic spacings in nanocrystalline Pd is not wider than the one in coarse-grained polycrystalline Pd. If the displacements of neighboring atoms were independent of each other, then the results would correspond to rms displacements from the lattice sites smaller by $1/\sqrt{2}$, that is the values for $\langle u_x^2 \rangle^{1/2}$ would be 0.052±0.004 and 0.052±0.007 Å, respectively.

As no significant deviation from the peak shape predicted for a Gaussian distribution of nearest-neighbor spacings is observed in Fig. 11, it is concluded that the peaks in the experimental atomic distribution function are related to the intragrain part of the total atomic distribution function, and that the distribution of nearest-neighbor interatomic spacings for the intergrain part of the atomic distribution function has a considerably larger width than the one of the intragrain part. In this case, the intergrain part of the atomic distribution function is a broad and shallow signal similar to a constant background, and the functional form of the peaks representing the lattice interatomic spacings (the intragrain part of the atomic distribution function) is unchanged. Due to the limited accuracy in the determination of $\langle \rho \rangle$ (compare Sec. III), the unstructured intergrain signal is not resolved in the experimental data. The qualitative difference between the narrow, Gaussian distributions of lattice interatomic spacings and the apparently much broader distribution of the nonlattice interatomic spacings is the reason why the two can be separated in the experimental analysis.

VI. CONCLUSIONS

A. Short-range order in the grain boundaries

The analysis of our atomic distribution function data for nanocrystalline Pd suggests the conclusion that there are two types of samples with a markedly different atomic structure, viz. those aged for more than 4 months or annealed, and those investigated within 10 days after preparation.

For aged or annealed samples, we find no indication for atoms on nonlattice sites. Our results suggest 4±3 atoms/nm^2, or 0.26±0.2 monolayers of atoms, on nonlattice grain-boundary sites, that is displaced by considerably more than 2.7% of the nearest-neighbor spacing. For interatomic spacings between atoms located in the same crystal, the root-mean-square deviation from the average nearest-neighbor interatomic spacing is not measurably increased as compared to the one of coarse-grained Pd. We have argued that the absence of a SRO peak in the intergrain part of the experimental atomic distribution functions indicates that on average over all grain boundaries, there is no preferred interatomic spac-

ing between atoms separated by a grain-boundary plane. Instead, the results suggest that the grain boundaries in the aged and annealed samples are similar to those of a simplistic nonreconstructed model of the grain boundary. In this model, highly ordered crystal lattices extend from both sides all the way to the mathematical plane of the grain boundary, where the defect is localized in an essentially two-dimensional manner, with a wide distribution of interatomic spacings across the plane.

This state of the grain boundaries appears to be different from the one implied by computer simulations of grain boundaries in conventional polycrystals. The simulations indicate that at least a fraction of an atomic monolayer of atoms in those grain boundaries is displaced sufficiently from their lattice positions to either be located outside of the coordination shell peaks (so that they would be detected as nonlattice atoms in the intragrain correlation function analysis) or else to induce a marked broadening of the coordination shell peaks. This is evident in the in-plane atomic distribution functions of the grain-boundary regions determined from computer simulation results.[45,13] No broadening of the peaks is detected in our experimental data, and the number of atoms on nonlattice positions is very small for the aged or annealed samples. Hence, it is questionable whether the atomic SRO in the grain boundaries in aged or annealed nanocrystalline Pd is the same as that in coarse-grained polycrystalline Pd. Future, detailed comparisons of the experimental data to computer simulations of the atomic structure of nanocrystalline materials, which are presently under way, are required in order to substantiate the presumed difference between the grain-boundary structures in aged and annealed nanocrystalline Pd on the one hand and in conventional polycrystalline materials on the other.

For as-prepared samples, the results indicate two clearly distinguished types of sites: lattice and nonlattice ones. At a grain size of the order of 10 nm, we find that about 10% of all atoms occupy nonlattice sites. For the lattice sites, the finding is again that the distribution of interatomic spacings is not measurably broadened as compared to that of the reference samples. In contrast to the case of the lattice sites, for which the rms deviation from the nearest-neighbor distance is small and similar to coarse-grained polycrystalline Pd, our results indicate that, on average over all grain boundaries in a sample, there is little or no atomic short-range order for the nonlattice sites. This finding may result from an extensive reconstruction of the atomic positions in the grain boundaries, which according to our results affects 1.8 ± 0.4 atomic monolayers.

There are several possible explanations for the different grain-boundary structures in the two types of samples. It is noted that the samples investigated immediately after preparation were also those with the smallest grain size. One may speculate upon a potential dependence of grain-boundary structure on grain size. As the lateral dimension of a grain boundary is reduced to a scale comparable to its structural units (e.g., the distance between intrinsic grain-boundary dislocations), it is not unreasonable to expect a qualitative change in the properties and in the structure of the grain boundary. However, as two samples, Pd03 and Pd07, with very similar fine grain size of $\langle D \rangle_{\text{area}} = 13$ and 12 nm, respectively, but different age (< 10 days and > 4 months, respectively), have different fractions of nonlattice atoms, the data appear in favor of age and thermal treatment, rather than grain size, as the factor responsible for the observed difference in atomic structure. Important grain growth was observed both during room-temperature aging and on annealing (compare Table I and Ref. 43). The atomic mobility required for grain growth to occur is expected to also allow for relaxation of the grain-boundary atomic structure. If relaxations upon aging (as opposed to grain size) are the decisive factor in determining the grain-boundary structure, then nanocrystalline palladium appears to be in a disordered state immediately after preparation, which then relaxes on a time scale of a few weeks towards the more ordered state observed in the aged or annealed samples. This would imply that the thermodynamic state of a nanocrystalline material is not uniquely determined by the microscopic variable grain size (or grain size distribution), but that there are additional degrees of freedom, similar to those which are responsible for the different thermodynamic states observed in glasses as a function of the quench rate, as opposed to the unique state of the undercooled melt. A recent calorimetric study of nanocrystalline platinum[16] arrives at the same conclusion.

The conclusion, in the present work, of scattering data as indicating "nonreconstructed" grain boundaries for aged or annealed, and highly disordered grain boundaries for as-prepared nanocrystalline Pd, compares to the interpretation of nanocrystalline Pd x-ray scattering data in terms of "ordered" grain boundaries in Ref. 4. In agreement with the conclusion in Ref. 4, the considerations in Sec. II C of the present study show that the absence of an observable diffuse background in the scattering pattern in Ref. 4 (indicating that the samples in the study may have been in the aged state) does indicate an ordered structure. We show that what is implied is specifically order in the sense that the outer atomic layers of each crystallite exhibit little or no reconstruction. On the other hand, we show that this quality and the absence of a diffuse background are compatible with a completely random distribution of interatomic spacings across the grain-boundary planes, implying the absence of correlations between the atomic positions on opposite sites of a grain-boundary plane. We have argued that the comparatively high perfection of the crystal lattice in nanocrystalline Pd is indicative of such a state of the grain boundaries.

The study demonstrates that the reduction in nearest-neighbor coordination number observed in EXAFS of nanocrystalline fcc and bcc metals is in at least qualitative agreement with x-ray scattering results. A comparative investigation applying both techniques to identical samples is in progress.

B. Short-range order in the crystal lattice

An experimental finding which deserves discussion is the unexpected result that coordination shells are not significantly broadened in nanocrystalline Pd as compared to those of the coarse-grained polycrystalline ma-

terial. The result is in apparent contradiction with data in the literature,[5] which show a temperature-independent additive contribution to the x-ray Debye-Waller parameter in nanocrystalline Pd, suggesting a contribution from static displacements to the rms distribution of displacements from the crystal lattice sites, $\langle u_x^2 \rangle^{1/2}$, in this material. At room temperature, the values for $\langle u_x^2 \rangle^{1/2}$ displacements determined in this way are 0.084 and 0.063 Å (3.1 and 2.3 % of the nearest neighbor spacing), respectively, in nanocrystalline Pd and coarse-grained polycrystalline Pd.[5] This is significantly larger than the value for $\langle u_x^2 \rangle^{1/2}$ determined from the atomic distribution functions in the present study, 0.052% for both nanocrystalline Pd and coarse-grained polycrystalline Pd. In agreement with our finding, a recent comparison of the EXAFS Debye-Waller parameters of *n*-Pd and coarse-grained Pd,[46] indicates a considerably smaller difference than the one implied by the x-ray Debye-Waller parameter. The different results reflect the fact that the x-ray atomic distribution and EXAFS results are sensitive to the SRO alone whereas the x-ray Debye-Waller parameter probes displacements from lattice sites on a scale of the grain size. Correlated atomic displacements, with neighboring atoms moving in the same direction, imply comparatively small deviations from the ideal nearest-neighbor distance, but significant displacements from the crystal lattice sites.[46–48] Therefore, the combined results of the different techniques indicate that the increased static part of the interference function Debye-Waller parameter observed in nanocrystalline Pd (Ref. 5) is due to displacement fields with a range of several interatomic spacings. Independent of the nature of the displacements, the experimental results suggest that the atomic SRO in the crystal lattice is affected little by the nm-scale structuring, whereas the SRO in the grain-boundary region may be strongly reduced.

C. Summary

In summary, we have presented a combined theoretical and experimental study of wide-angle scattering by nanocrystalline solids. From theoretical considerations, we conclude that for crystallites with a random distribution of lattice orientation, unless a significant fraction of atoms are displaced from their lattice sites, the wide-angle interference function of a poly- or nanocrystalline solids is identical to that of an arrangement of isolated particles with the same size or size distribution as those of the poly- or nanocrystalline solid. Our experimental data confirm the theoretical prediction that in nanocrystalline solids the relative reduction in crystal lattice coordination number increases linearly with interatomic distance. The experimental results show that, as a function of sample age and/or grain size, different types of reduction in coordination number are observed in nanocrystalline Pd: for aged or annealed samples the relative reduction in coordination numbers vanishes upon extrapolation to zero interatomic distance, indicating that essentially all atoms are located on crystal lattice sites, and that the topological defect is localized in the two-dimensional grain-boundary plane, similar to a simplistic nonreconstructed grain-boundary model. For samples investigated immediately after preparation, the extrapolated relative reduction in coordination number is finite, indicating a significant fraction of atoms on nonlattice sites. The results imply that there is little short-range order for the nonlattice atoms. Therefore, the results suggest that the grain-boundary atomic structure in as-prepared nanocrystalline Pd differs qualitatively from the more ordered one of coarse-grained polycrystalline material. In contrast to the disordered grain-boundary component, no reduction in short-range order is observed in the atomic distribution function of the crystal lattice component, indicating that disorder in the crystal lattice involves displacements correlated over several lattice parameters, rather than short-range, uncorrelated atomic displacements.

ACKNOWLEDGMENTS

The authors acknowledge stimulating discussions with R. Birringer, H. Gleiter, and C. E. Krill. We are indebted to H. Gleiter for encouragement to carry out this work and for generous support. This project was supported by Deutsche Forschungsgemeinschaft (G.W. Leibniz Programm H. Gleiter). Support by Alexander von Humboldt Foundation (J.W.) and Studienstiftung des deutschen Volkes (J.L.) is gratefully acknowledged.

APPENDIX: RELATING THE INTRAGRAIN CORRELATION FUNCTION TO THE PARTICLE SURFACE

The correlation function H at small interatomic distance r is expected to be related to the particle surface A, because for small r only atoms located in volume elements closer than r to a surface experience a reduction in coordination number. The number of those volume elements increases with r and with A. In the limit $r \rightarrow 0$, r is much smaller than the radius of curvature of the particle surface practically everywhere, so the surface can be assumed plane. In this case, it is advantageous to express H as the sum of two functions $H_{1(r)}$ and $H_{2(r)}$, where $H_{1(r)}$ is the contribution of those volume elements which are not affected by the presence of the surface (i.e., those which are farther away from the surface than r, the hatched region labeled V_1 in Fig. 13), with a total

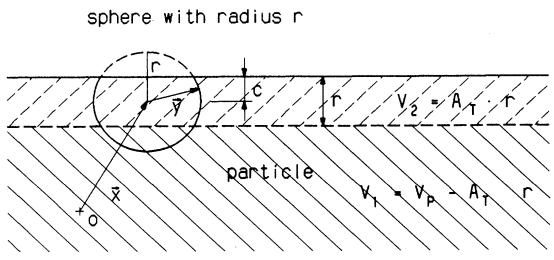

FIG. 13. Schematic illustration of the geometrical construction used to evaluate the relative reduction in nearest-neighbor coordination number at interatomic distance r for an atom located C below a plane surface. Hatched regions, particle volume; atoms located in V_1 have full coordination numbers, atoms located in V_2 have reduced coordination numbers.

volume $V_1 = V^P - Ar$, and $H_{2(r)}$ is the contribution of the remaining elements, occupying a volume $V_2 = Ar$ (the hatched region labeled V_2 in Fig. 13). For both regions, $H_{(r)}$ can be determined as the average, over all points inside the particle, of that fraction of a spherical shell of radius r, centered at the point, which is contained inside the particle (see Sec. II B).

Since the whole shell is contained inside the particle for each point in V_1, we have simply

$$H_{1(r)} = \frac{V_1}{V^P} = 1 - \frac{Ar}{V^P} . \tag{A1}$$

On the other hand, a shell centered around a point in V_2 will only in part be contained inside the particle. For an atom located at a depth C below the surface, the fraction of the shell (radius r) outside the particle is $M_{(r,C)}/4\pi r^2$, where $M_{(r,C)}$ is the area of a spherical cap with radius r and height $r - C$ (see Fig. 13). Hence,

$$H_{2(r)} = \frac{A}{V^P} \int_{C=0}^{r} \left[1 - \frac{M_{(r,C)}}{4\pi r^2} \right] dC = \frac{3Ar}{4V^P} \tag{A2}$$

and, since $H = H_1 + H_2$, the required result for the variation of H at small r is

$$H_{(r)} = 1 - \frac{A}{4V^P} r \quad (r \to 0) . \tag{A3}$$

---

*Present address: Paul Scherrer Institut, CH-5232 Villigen-PSI, Switzerland.

†Present address: National Institute of Standards and Technology, 223/B152, Gaithersburg, MD 20899.

[1]H. Gleiter, in *Proceedings of the Second Risø International Symposium on Metallurgy and Materials Science,* edited by N. Hansen, T. Leffers, and H. Lilholt) (Røskilde, Denmark, 1981), pp. 15–21.

[2]R. Birringer, H. Gleiter, H.-P. Klein, and P. Marquardt, Phys. Lett. **102A**, 365 (1984).

[3]X. Zhu, R. Birringer, U. Herr, and H. Gleiter, Phys. Rev. B **35**, 9085 (1987).

[4]M. R. Fitzsimmons, J. A. Eastman, M. Müller-Stach, and G. Wallner, Phys. Rev. B **44**, 2452 (1991).

[5]J. A. Eastman, M. R. Fitzsimmons, and L. J. Thompson, Philos. Mag. B **66**, 667 (1992).

[6]T. Haubold, R. Birringer, B. Lengeler, and H. Gleiter, Phys. Lett. A **135**, 461 (1989).

[7]T. Haubold, W. Krauss, and H. Gleiter, Philos. Mag. Lett. **63**, 245 (1991).

[8]H. E. Schäfer, W. Eckert, O. Stritzke, R. Würschum, and W. Templ, in *Positron Annihilation,* edited by L. Dorikens-Vanpraet, M. Dorikens, and D. Seegers (World Scientific, Singapore, 1989), pp. 79–85.

[9]G. J. Thomas, R. W. Siegel, and J. A. Eastman, Scr. Met. **24**, 201 (1990).

[10]W. Wunderlich, I. Ishida, and R. Maurer, Scr. Met. **24**, 403 (1990).

[11]J. Weissmüller, R. Birringer, and H. Gleiter, in *Microcomposite and Nanophase Materials,* edited by D. C. Van Aken, G. S. Was, and A. K. Gosh (TMS, Warrendale, PA, 1991), pp. 1–14.

[12]N. Schlorke, J. Weissmüller, W. Dickenscheid, and H. Gleiter, Nanostruct. Mater. **6**, 593 (1995).

[13]D. Wolf, in *Materials Interfaces,* edited by D. Wolf and S. Yip (Chapman and Hall, London, 1992), pp. 87–150.

[14]H.-J. Höfler, Ph.D. thesis, Universität des Saarlandes, Saarbrücken, Germany, 1991.

[15]B. Günther, A. Kumpmann, and H.-D. Kunze, Scr. Met. **27**, 833 (1992).

[16]A. Tschöpe, R. Birringer, and H. Gleiter, J. Appl. Phys. **71**, 5391 (1992).

[17]C. E. Krill and R. Birringer (unpublished).

[18]J. Weissmüller, J. Löffler, C. E. Krill, R. Birringer, and H. Gleiter (unpublished).

[19]M. Celino, G. D'Agostino, and W. Rosato, Nanostruct. Mater. **6**, 751 (1995).

[20]D. Wolf, J. Wang, S. R. Phillpot, and H. Gleiter, Phys. Rev. Lett. **74**, 4686 (1995).

[21]H. Zhu and R. S. Averback, Mater. Sci. Eng. (to be published).

[22]The same quantity is also referred to in the literature as atomic density distribution function, pair distribution function, pair density function, or radial distribution function.

[23]L. Azárroff, R. Kaplow, N. Kato, R. Weiss, A. Wilson, and R. Young, *X-Ray Diffraction* (McGraw-Hill, New York, 1974), Sec. 2.

[24]In the present work, scattering is discussed in terms of the interference function $P(k)$ (Ref. 23) as opposed to a quantity which is more commonly referred to in the literature, the structure factor $S(k)$. The two quantities are related by $S(k) = P(k) + 1$. The use of the interference function as opposed to the structure factor simplifies the equations in Secs. II B and II E. Note also, that in the present work the symbol S is used to designate the small-angle part of the interference function [Eqs. (9) and (11)].

[25]G. Porod, in *Small-Angle X-ray Scattering,* edited by O. Glatter and O. Krattky (Academic, London, 1982).

[26]H. Hermann, Mater. Sci. Forum **78**, 1 (1991).

[27]Note that α_S refers to a hypothetical free surface area, which corresponds to the true free surface area only when there is no contact between the crystallites.

[28]F. Bertaut, Acta Crystallogr. **3**, 14 (1950).

[29]F. Betts and A. Bienenstock, J. Appl. Phys. **43**, 4591 (1972).

[30]M. R. Fitzsimmons and S. L. Sass, Acta Metall. **36**, 3103 (1988).

[31]M. S. Taylor, I. Majid, P. D. Bristowe, and R. W. Baluffi, Phys. Rev. B **40**, 2772 (1989).

[32]I. Majid, P. D. Bristowe, and R. W. Baluffi, Phys. Rev. B **40**, 2779 (1989).

[33]O. Glatter, J. Appl. Phys. **13**, 7 (1980).

[34]B. E. Warren, *X-Ray Diffraction* (Dover, New York, 1990), Chap. 13.

[35]R. Birringer, H. Gleiter, H.-P. Klein, and P. Marquardt, Phys. Lett. **102A**, 365 (1984).

[36]H. Gleiter, Prog. Mater. Sci. **33**, 223 (1989).

[37]C. N. J. Wagner, J. Non-Cryst. Solids **42**, 3 (1980).
[38]L. Schwartz and J. Cohen, *Diffraction from Materials* (Springer-Verlag, Berlin, 1987).
[39]J. Weissmüller, J. Non-Cryst. Solids **142**, 70 (1992).
[40]L. Azárroff, R. Kaplow, N. Kato, R. Weiss, A. Wilson, and R. Young, *X-Ray Diffraction* (McGraw-Hill, New York, 1974), Sec. 2.II.F.
[41]M. A. Krivoglaz, *Theory of X-Ray and Thermal Neutron Scattering by Real Crystals* (Plenum, New York, 1969), Sec. 23.
[42]More precisely, the Debye-Waller factor is determined by the rms of the projection of the atomic displacements on the scattering vector. However, in an isotropic sample the rms displacement is identical along any spatial direction and therefore the orientation of the coordinate system is irrelevant.
[43]J. Weissmüller, J. Löffler, and M. Kleber, Nanostruct. Mater. **6**, 105 (1995).
[44]H. P. Klug and L. E. Alexander, *X-Ray Diffraction Procedures for Polycrystalline and Amorphous Materials,* 2nd ed. (Wiley, New York, 1974).
[45]D. Wolf and J. F. Lutsko, Phys. Rev. Lett. **60**, 1170 (1988).
[46]F. Boscherini, in *Proceedings of the 1993 CNR School on Nanostructured Materials,* edited by D. Fiorani (World Scientific, Singapore, 1993).
[47]G. Beni and P. Platzmann, Phys. Rev. B **14**, 1514 (1976).
[48]A. Balerna and S. Mobilio, Phys. Rev. B **34**, 2293 (1986).